ChemComm

COMMUNICATION

View Article Online
View Journal | View Issue

Cite this: *Chem. Commun.*, 2023, 59, 12431

Received 29th August 2023,
Accepted 22nd September 2023

DOI: 10.1039/d3cc04235a

rsc.li/chemcomm

Observation of an electron-precise metal boryne complex: $[Bi{\equiv}BH]^-$†

Han-Wen Gao, Jie Hui and Lai-Sheng Wang *

Metal-boron triple bonds are rare due to the electron deficiency of boron. This study uncovers a simple electron-precise metal boryne complex, $[Bi{\equiv}BH]^-$, which is produced within an ion trap through chemical reactions of the open-shell BiB^- anion with H_2. Photoelectron imaging is used to investigate the electronic structure and chemical bonding of the $BiBH^-$ complex. The B atom in the linear closed-shell $BiBH^-$ is found to undergo sp hybridization, forming a B–H single bond and a Bi≡B triple bond. Photoelectron imaging reveals three detachment transitions from the $BiBH^-$ ($^1\Sigma^+$) anion to the neutral BiBH, including the ground state ($^2\Pi_{3/2}$) and two excited states ($^2\Sigma^+$ and $^2\Pi_{1/2}$). Strong vibronic coupling is observed between the $^2\Pi_{3/2}$ and $^2\Sigma^+$ states, evidenced by the appearance of bending vibrations and their unique photoelectron angular distributions. The $BiBH^-$ complex not only stands as the simplest metal boryne complex, but also serves as an ideal molecular system to investigate both spin–orbit and vibronic couplings.

Transition metal carbyne complexes constitute an important class of organometallic compounds which have wide applications as catalysts in organic chemistry and the pharmaceutical industry.[1–4] However, metal boryne complexes are much rarer due to boron's electron deficiency, despite the fact that borylene chemistry has been well developed.[5–8] There are three ways that boron can form a triple bond by compensating its electron deficiency: (1) through coordination by an electron pair of a donor ligand, (2) through back donation of a transition metal, or (3) accepting an electron in a formal B^- center, which is isoelectronic to the carbon atom.[9] The first diboryne complex was observed in a low temperature matrix through the coordination of two CO molecules in $[OC{\rightarrow}B{\equiv}B{\leftarrow}CO]$.[10] The first stable diboryne compound synthesized in macroscopic quantity was protected by two bulky carbene ligands $[L{\rightarrow}B{\equiv}B{\leftarrow}L]$ [L = 1,3-bis(2,6-diisopropylphenyl)imidazol-2-ylidene].[11] Back donation from a transition metal to boron has even led to the formation of a M≡B quadrupole bond in Rh≡B, $(BO^-)Rh{\equiv}B$, and $B{\equiv}Fe(CO)_3^-$.[12,13] The protonation of RhB breaks the quadrupole bond and gives rise to a simple metal boryne cation, $[Rh{\equiv}BH]^+$, which was studied computationally to verify the quadrupole bond in Rh≡B.[12] The boronyl-coordinated diboryne $[OB\text{-}B{\equiv}B\text{-}BO]^{2-}$ can be considered to contain two B^- centers, which undergo sp hybridization.[14] Similarly, the first metal boron triple bond in $[Bi{\equiv}B\text{-}BO]^-$ should also be considered to contain an sp-hybridized B^- center.[15] Several transition metal boryne complexes have been produced using the similar formula $[M{\equiv}B\text{-}BO]^-$,[16] as well as $[Pb{\equiv}B\text{-}BO]^{2-}$,[17] which is isoelectronic to $[Bi{\equiv}B\text{-}BO]^-$. In this Communication, we report the experimental observation of the simplest metal boryne complex $[Bi{\equiv}BH]^-$, which contains an sp-hybridized B^- center, and its characterization using photoelectron imaging. While the metal-boron triple bond in the $[M{\equiv}B\text{-}BO]^-$ type of complexes may have conjugation effects with the BO ligand, the simple $[Bi{\equiv}BH]^-$ boryne complex provides an opportunity to directly examine the metal-boron triple bond.

The experiment was carried out using a high-resolution photoelectron imaging apparatus consisting of a cryogenically-controlled Paul trap.[18] The $[BiBH]^-$ complex was discovered serendipitously during our experiment on Bi-doped boron clusters,[19] which were produced using laser vaporization of a composite target made of Bi and ^{10}B- or ^{11}B-enriched powders. The laser-induced plasma was quenched by a helium carrier gas, initiating nucleation to form $Bi_xB_y^-$ mixed clusters. The nascent clusters were entrained in the carrier gas and underwent a supersonic expansion. After passing a skimmer, the collimated cluster beam was sent directly into a cryogenically-cooled Paul trap operated at 4.2 K. The cluster anions were trapped and cooled collisionally by a mixed He/H_2 buffer gas (4 : 1 by volume) for 45 ms before being pulsed into the extraction region of a time-of-flight (TOF) mass spectrometer. In the mass region of BiB^-, a very weak $BiBH^-$ impurity mass signal was observed, most likely due to a trace amount of water contaminant on the target surface.

Department of Chemistry, Brown University, Providence, RI 02912, USA.
E-mail: lai-sheng_wang@brown.edu

† Electronic supplementary information (ESI) available. See DOI: https://doi.org/10.1039/d3cc04235a

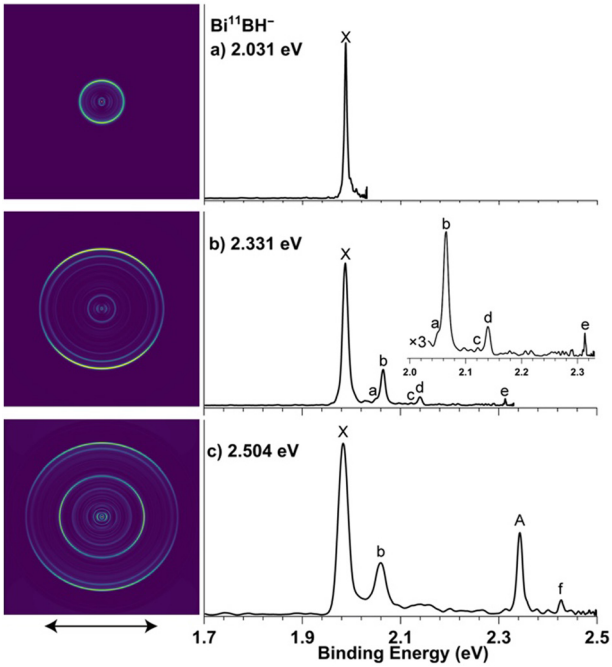

Fig. 1 Photoelectron images and spectra of cryogenically-cooled $Bi^{11}BH^-$ taken at (a) 2.031 eV (610.55 nm), (b) 2.331 eV (531.89 nm), and (c) 2.504 eV (495.21 nm). The double arrow below the image indicates the laser polarization. The inset in (b) is intended to show the weak features *a* and *c*.

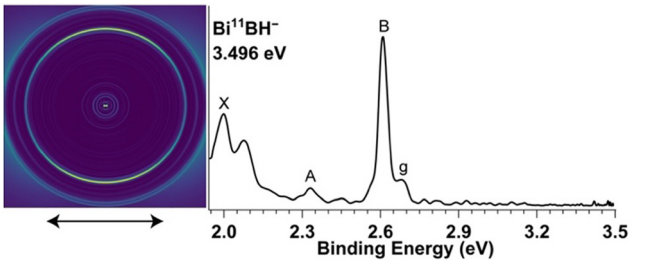

Fig. 2 The photoelectron image and spectrum of cryogenically-cooled $Bi^{11}BH^-$ taken at 3.496 eV (355 nm). The double arrow below the image indicates the laser polarization.

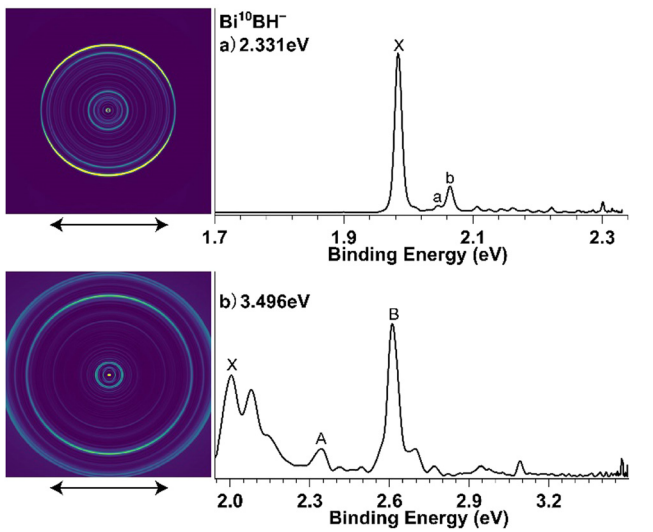

Fig. 3 Photoelectron images and spectra of cryogenically-cooled $Bi^{10}BH^-$ taken at (a) 2.331 eV (531.89 nm) and (b) 3.496 eV (355 nm). The double arrow below the image indicates the laser polarization.

Surprisingly, the $BiBH^-$ mass signal was significantly enhanced after cooling and trapping, as shown in Fig. S1 (ESI†), where the mass spectra with and without ion trapping are compared. Apparently, the open-shell BiB^- anion[19c] can react with the H_2 cooling gas in the ion trap to form the closed-shell $BiBH^-$ anion. We suspect that the chemical reaction takes place during the initial ion trapping, when the cluster beam still carries a high kinetic energy. Thus, energetic collisions between the open-shell BiB^- and H_2 could overcome the expected reaction barrier to form $BiBH^-$, which was subsequently cooled in the ion trap. The ion trapping slightly increases the mass resolution, as shown in Fig. S1 (ESI†), because the ion packet upon extraction from the ion trap is focused to a smaller volume into the extraction zone of the TOF mass spectrometer.[18] More experimental details can be found in the ESI.†

Fig. 1 displays high-resolution photoelectron images and spectra at three photon energies (2.031, 2.331, 2.504 eV) for the cryogenically-cooled $Bi^{11}BH^-$. Two electronic transitions (X and A) are observed, each with vibrational fine features labeled by lower case letters. Fig. 2 shows the photoelectron image and spectrum of cold $Bi^{11}BH^-$ at 3.496 eV photon energy, revealing one more detachment transition (peak B) with one vibrational fine feature (peak g). We also conducted experiments on the $Bi^{10}BH^-$ isotopomer at 2.331 eV and 3.496 eV photon energies, as displayed in Fig. 3. Because the isotopically-enriched boron powders had a 97% isotope purity, the spectra of $Bi^{10}BH^-$ always contain weak signals of $Bi^{11}B^-$ as a minor contaminant (Fig. 3).[19c] On the other hand, the $Bi^{11}BH^-$ isotopomer does not have any potential ^{10}B-contaminant. Thus, we have focused on the $Bi^{11}BH^-$ isotopomer, but the $Bi^{10}BH^-$ data are valuable to verify the assignment of the vibrational structures in the $Bi^{11}BH^-$ spectra.

Peak X in Fig. 1a for $Bi^{11}BH^-$ has a clear s + d wave angular distribution. It should be the 0–0 transition to the ground electronic state of BiBH and defines an accurate electron affinity (EA) of 1.988 ± 0.001 eV for BiBH. In Fig. 1b, three prominent vibrational features (peaks b, d, e) following peak X are observed. Peaks X, b and d can be easily recognized as one vibrational progression because they have the same energy spacing and they have the same s + d wave angular distribution, yielding a vibrational frequency of 613 cm^{-1} for $Bi^{11}BH$. The corresponding frequency for $Bi^{10}BH$ is 649 cm^{-1}, measured from peak b in Fig. 3a. There is a weak shoulder (a) on the lower binding energy side of peak b in Fig. 1b, but it is not well resolved. The corresponding feature (a) is well separated from peak b in the spectrum of $Bi^{10}BH^-$ (Fig. 3a). It is surprising that peak a in the spectra of both isotopomers has a p-wave angular distribution, different from that of peak X and the other two

vibrational peaks b and d. Following peak a, the second quantum of this vibration is discernible (peak c, Fig. 1b), which also carries a p-wave angular distribution. Peaks a and c yield a vibrational frequency of 540 cm^{-1} for $Bi^{11}BH$. This frequency is 499 cm^{-1} for $Bi^{10}BH$, defined by peak a (Fig. 3a). Peak e with an s + d wave angular distribution (Fig. 1b) should represent a high frequency vibrational mode, yielding a frequency of 2621 cm^{-1}. Weak vibrational features are more difficult to identify in the spectra of the $Bi^{10}BH^-$ isotopomer (Fig. 3) because of the contamination of $Bi^{11}B^-$, as mentioned above.

As the photon energy increases to 2.504 eV (Fig. 1c), the stronger peak A with a p-wave angular distribution should be the first excited state of $Bi^{11}BH$. Peak f should represent a vibrational progression of peak A, yielding a vibrational frequency of 675 cm^{-1}. However, peak f carries an s + d wave angular distribution, different from that of peak A. No other vibrational progression is observed off peak A. The highest photon energy spectrum at 3.496 eV (Fig. 2) reveals an intense peak B, which should be the second excited state of $Bi^{11}BH$. A vibrational feature (peak g) is also observed, yielding a vibrational frequency of 573 cm^{-1}. Both peaks B and g carry s + d wave angular distributions. The different angular distributions of peaks a and f from their respective electronic states are intriguing, suggesting that they have different symmetries from the parent electronic states. They should be due to the bending modes, which are not symmetry-allowed if both $BiBH^-$ and BiBH are linear. Their appearance can also be due to strong vibronic coupling between the ground state and the first excited state mediated by the bending mode. Hence, the 540 cm^{-1} frequency for the ground state from Fig. 1b should be due to the bending mode; and the 613 cm^{-1} and 2621 cm^{-1} frequencies should be due to the Bi–B and B–H stretching modes for $Bi^{11}BH$, respectively. The binding energies of the observed photoelectron features, their β parameters (see ESI†), and assignments are given in Table S1 (ESI†).

We optimized the structure of $BiBH^-$ using density functional theory (DFT) at the PBE0/aug-cc-pVTZ level[20] using Gaussian 09[21] and found that the ground state of $BiBH^-$ is linear with $C_{\infty v}$ symmetry (Fig. 4a) and a closed-shell electron configuration ($^1\Sigma^+$). The triplet state was found to be at least 2 eV higher in energy. The valence molecular orbitals (MOs) of $BiBH^-$ are shown in Fig. 4b. The highest occupied MO (HOMO) is a π bonding orbital between Bi and B. The HOMO−1 is mainly a σ bonding orbital between Bi and B, whereas the HOMO−2 is mainly a σ bonding orbital between B and H. The HOMO−3 is mainly the Bi 6*s* lone pair. Electron detachment from the HOMO results in the open-shell ground state of BiBH, $3\sigma^2 1\pi^3$ ($^2\Pi_{3/2}$, $^2\Pi_{1/2}$). Large spin–orbit coupling is expected and the ground state of BiBH should be $^2\Pi_{3/2}$, corresponding to the X band in the photoelectron spectra. The s + d wave angular distribution of the X band is consistent with electron detachment from a π orbital. On the basis of its s + d wave angular distribution, the B band should correspond to the $^2\Pi_{1/2}$ state, giving rise to a large spin–orbit splitting of 0.622 eV (Table S1, ESI†). The A band then must correspond to the $^2\Sigma^+$ ($3\sigma^1 1\pi^4$) excited state of BiBH, derived from detachment of a 3σ electron, consistent with the p-wave angular distribution. The strong spin–orbit coupling should suppress the Renner–Teller effect in the $^2\Pi$ state of BiBH.[22] However, the observation of the bending modes in the $^2\Pi_{3/2}$ and $^2\Sigma^+$ states and their unique angular distributions (peaks a, c, f in Fig. 1 and Table S1, ESI†) suggest vibronic coupling between the $^2\Pi_{3/2}$ and $^2\Sigma^+$ states. The small energy difference between these two states makes vibronic coupling possible.

We analyzed the chemical bonding of $BiBH^-$ using the AdNDP method,[23] as shown in Fig. S2 (ESI†). We can clearly see the two π bonds and the σ bond between Bi and B, and the σ bond between B and H. Because of the relativistic stabilization,[24] the 6s electrons of Bi are known to be inert and form a lone pair, found in all Bi-containing boron clusters.[15,19,25] The B atom undergoes sp hybridization, where one of the sp hybridized orbitals forms the σ bond with the H 1s orbital and the other forms a σ bond with the $6p_z$ orbital of Bi. The $2p_x$ and $2p_y$ orbitals of B form the π bonds with the $6p_x$ and $6p_x$ orbitals of Bi, giving rise to the Bi≡B triple bond. We performed Wiberg bond order analyses and found that the bond order between Bi and B is 2.89, which agrees well with the triple bond. The calculated Bi–B bond length of 2.049 Å agrees well with that (2.08 Å) estimated using the triple bond covalent radii from Pyykko.[26] The Bi–B triple bond length in $BiBH^-$ is similar to the Bi–B triple bond length of 2.036 Å computed for $[Bi{\equiv}B{-}B{\equiv}O]^-$ at the same level of theory (PBE0/aug-cc-pVTZ).[15]

In the BiBH neutral, one π electron is removed, weakening the Bi–B bond and leaving a bond order of 2.5 for Bi–B. Thus, the measured Bi–B stretching frequency of 613 cm^{-1} for $Bi^{11}BH$ (649 cm^{-1} for $Bi^{10}BH$) is expected to be lower than that of the anions. The contribution of the Bi 6p orbitals to the π bonding in BiBH can be estimated using the measured spin–orbit splitting between $^2\Pi_{3/2}$ and $^2\Pi_{1/2}$,[27] as are shown in the ESI.† We found that the Bi 6p orbitals contribute about 50% to the π bonds. We also calculated the atomic compositions of the π orbitals and found that the Bi 6p orbitals contribute about 60% to the π bonds, consistent with the estimation using the measured spin–orbit splitting. Both methods provide strong evidence for the covalent nature of the bonding between Bi and B. Our computed Bi–B stretching frequency for the $Bi^{11}BH^-$

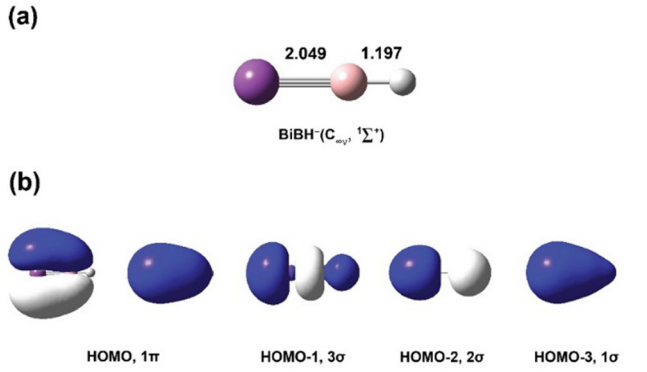

Fig. 4 The structure (a) and valence molecular orbitals (b) of $BiBH^-$ at the PBE0/aug-cc-pVTZ level.

anion is 710 cm^{-1} (739 cm^{-1} for the $Bi^{10}BH^-$ isotopomer), indicating a relatively strong bond. This Bi–^{10}B stretching frequency is slightly larger than that for Au–^{10}B (710 cm^{-1}), which is known to contain an Au≡B triple bond.[28] It should be noted that a previous computational study considered the substituent effects on the Bi≡B triple bond in R-Bi≡B-R type neutral complexes.[29] However, in these complexes the Bi 6s electrons are needed in the chemical bonding. In light of the inertness of the 6s electron pair, we think that $[Bi{\equiv}B\text{-}R]^-$ type anionic complexes may be more promising targets for syntheses if suitable R groups and counter ions can be found.

In conclusion, we report the formation of an electron-precise metal boryne complex $[Bi{\equiv}BH]^-$ through chemical reactions of BiB^- with H_2 in a cryogenically-cooled ion trap. The electronic structure and chemical bonding of the closed-shell $[Bi{\equiv}BH]^-$ are investigated using high-resolution photoelectron imaging. The electron affinity of neutral BiBH ($^2\Pi_{3/2}$) is measured to be 1.988(1) eV, along with two excited states, $^2\Sigma^+$ at an excitation energy of 0.355 eV and $^2\Pi_{1/2}$ at an excitation energy of 0.622 eV. Vibronic coupling between the $^2\Pi_{3/2}$ ground state and the $^2\Sigma^+$ excited state is observed. Chemical bonding analysis reveals a Bi≡B triple bond in the electron-precise $[Bi{\equiv}BH]^-$, in which the B atom undergoes sp hybridization. The $[Bi{\equiv}BH]^-$ anionic species represents the simplest metal boryne complex characterized experimentally. The current study demonstrates the intriguing possibility that the ion trap can be used to form other metal boryne complexes or other hydrogen stabilized clusters.

This work was supported by the National Science Foundation (Grant No. CHE-2053541).

Conflicts of interest

There are no conflicts to declare.

Notes and references

1 E. O. Fischer, G. Kreis, C. G. Kreiter, J. Muller, G. Huttner and H. Lorenz, *Angew. Chem., Int. Ed. Engl.*, 1973, **12**, 564.
2 R. R. Schrock, *Science*, 1983, **219**, 13.
3 J. W. Herndon, *Coord. Chem. Rev.*, 2005, **249**, 999.
4 R. R. Schrock, *Angew. Chem., Int. Ed.*, 2006, **45**, 3748.
5 H. Braunschweig, C. Kollann and U. Englert, *Angew. Chem., Int. Ed.*, 1998, **37**, 3179.
6 D. Vidovic, G. A. Pierce and S. Aldridge, *Chem. Commun.*, 2009, 1157.
7 H. Braunschweig, R. D. Dewhurst and V. H. Gessner, *Chem. Soc. Rev.*, 2013, **42**, 3197.
8 M. Soleihavoup and G. Bertrand, *Angew. Chem., Int. Ed.*, 2017, **56**, 10282.
9 J. K. Olson and A. I. Boldyrev, *Chem. Phys. Lett.*, 2012, **523**, 83.
10 M. Zhou, N. Tsumori, Z. Li, K. Fan, L. Andrews and Q. Xu, *J. Am. Chem. Soc.*, 2002, **124**, 12936.
11 H. Braunschweig, R. D. Dewhurst, K. Hammond, J. Mies, K. Radacki and A. Vargas, *Science*, 2012, **336**, 1420.
12 L. F. Cheung, T. T. Chen, G. S. Kocheril, W. J. Chen, J. Czekner and L. S. Wang, *J. Phys. Chem. Lett.*, 2020, **11**, 659.
13 C. Chi, J. Q. Wang, H. S. Hu, Y. Y. Zhang, W. L. Li, L. Meng, M. Luo, M. Zhou and J. Li, *Nat. Commun.*, 2019, **10**, 4713.
14 S. D. Li, H. J. Zhai and L. S. Wang, *J. Am. Chem. Soc.*, 2008, **130**, 2573.
15 T. Jian, L. F. Cheung, T. T. Chen and L. S. Wang, *Angew. Chem., Int. Ed.*, 2017, **56**, 9551.
16 (*a*) T. T. Chen, L. F. Cheung, W. J. Chen, J. Cavanagh and L. S. Wang, *Angew. Chem., Int. Ed.*, 2020, **59**, 15260; (*b*) T. T. Chen, L. F. Cheung and L. S. Wang, *Annu. Rev. Phys. Chem.*, 2022, **73**, 233.
17 W. J. Chen, T. T. Chen, Q. Chen, H. G. Lu, X. Y. Zhao, Y. Y. Ma, Q. Q. Yan, R. N. Yuan, S. D. Li and L. S. Wang, *Commun. Chem.*, 2022, **5**, 25.
18 (*a*) G. S. Kocheril, H. W. Gao, D. F. Yuan and L. S. Wang, *J. Chem. Phys.*, 2022, **157**, 171101; (*b*) G. S. Kocheril, H. W. Gao and L. S. Wang, *Mol. Phys.*, 2023, e2182610; (*c*) G. S. Kocheril, H. W. Gao and L. S. Wang, *J. Chem. Phys.*, 2023, **158**, 236101.
19 (*a*) L. F. Cheung, J. Czekner, G. S. Kocheril and L. S. Wang, *J. Chem. Phys.*, 2019, **150**, 064304; (*b*) W. J. Chen, M. Kulichenko, H. W. Choi, J. Cavanagh, D. F. Yuan, A. I. Boldyrev and L. S. Wang, *J. Phys. Chem. A*, 2021, **125**, 6751; (*c*) H. W. Gao, H. W. Choi, J. Hui, W. J. Chen, G. S. Kocheril and L. S. Wang, *J. Chem. Phys.*, 2023, **159**, 114301.
20 C. Adamo and V. Barone, *J. Chem. Phys.*, 1999, **110**, 6158.
21 M. J. Frisch *et al.*, *Gaussian 09, Revision A.1*, Gaussian, Inc., Wallingford, CT, 2009.
22 S. Mishra, V. Vallet, L. V. Poluyanov and W. Domcke, *J. Chem. Phys.*, 2006, **124**, 044317.
23 D. Y. Zubarev and A. I. Boldyrev, *Phys. Chem. Chem. Phys.*, 2008, **10**, 5207.
24 P. Pyykko, *Chem. Rev.*, 1988, **88**, 563.
25 T. Jian, G. V. Lopez and L. S. Wang, *J. Phys. Chem. B*, 2016, **120**, 1635.
26 P. Pyykko, *J. Phys. Chem. A*, 2015, **119**, 2326.
27 H. Lefebvre-Brion and R. W. Field, *The Spectra and Dynamics of Diatomic Molecules*, Elsevier, Boston, 2004.
28 L. F. Cheung, G. S. Kocheril, J. Czekner and L. S. Wang, *J. Chem. Phys.*, 2020, **152**, 174301.
29 J. S. Lu, S. H. Su, M. C. Yang, X. T. Wen, J. Z. Xie and M. D. Su, *Organometallics*, 2016, **35**, 3924.

